communications chemistry

Article

https://doi.org/10.1038/s42004-024-01246-8

Non-threaded and rotaxane-type threaded wheel–axle assemblies consisting of dinickel(II) metallomacrocycle and dibenzylammonium axle

Yoko Sakata[1,3], Seiya Kobayashi[1], Misato Yamamoto[1], Katsuya Doken[1], Mayu Kamezawa[1], Sachiko Yamaki[2] & Shigehisa Akine[1,2] ✉

Rotaxanes are typically prepared using covalent bonds to trap a wheel component onto an axle molecule, and rotaxane-type wheel–axle assembly using only noncovalent interactions has been far less explored. Here we show that a dinickel(II) metallomacrocycle forms two different types of wheel–axle assemblies with a dibenzylammonium axle molecule based only on noncovalent interactions. The non-threaded assembly was obtained by introduction of Ni^{2+} into the macrocycle before the complexation with the axle molecule (metal-first method). The non-threaded assembly was in rapid equilibrium with each of the components in solution. The threaded assembly was obtained by introduction of Ni^{2+} after the formation of a pseudorotaxane from the non-metalated wheel and the axle molecule (axle-first method). The threaded assembly was not in equilibrium with the dissociated species even though it was maintained only by noncovalent interactions. Thus, formation of one of the non-threaded and threaded wheel–axle assemblies over the other is governed by the assembly pathway.

Rotaxanes are mechanically interlocked molecules in which a molecular wheel is trapped on a dumbbell-shaped axle[1–4]. To date, various kinds of rotaxanes have been synthesized and used as components of molecular machines[5–12], catalysts[13–20], entangled polymer materials[21–31], etc. In principle, the synthesis of rotaxanes requires rational strategies to suitably assemble the wheel and axle components before interlocking; the typical and well-established methods include capping and clipping.

In order to make a rotaxane structure consisting of a wheel and an axle component, two different types of interactions/bonds are necessary; one is to preassemble the two components and the other is to lock the preassembled structure. In general, noncovalent interactions are used for the preassembly, while covalent bond formation is used in the second step for complete interlocking, e.g., introduction of bulky stoppers in the capping method and ring closure in the clipping method. However, noncovalent interactions have also been used for interlocking when these have a less reversible feature. In fact, there have been various rotaxane structures containing metal atoms in the wheel and/or axle components[32–38]. In some of these structures, the metal constituents are essential, because the interlocked rotaxane structures cannot be maintained without the metal atoms. For example, the metal atoms are introduced at both ends of the axle as a part of the stopper groups[39–42], at the center of the axle as the interacting motif with the wheel[43–48], or in the wheel as the constituent metal to complete the metallomacrocycle[49–53]. These metal-containing rotaxanes are obtained by coordination-based capping and clipping, which keeps the wheel and axle interlocked[39–42,49–53]. Shrinking is also a unique method to obtain an interlocked rotaxane structure from the corresponding preassembled components or to control the shuttling motions[54–57]. For example, a pseudorotaxane is converted into a genuine rotaxane by incorporating metal ions into the coordination sites of the wheel component while keeping the axle threaded[54]. In general, intermolecular association based on noncovalent interactions produces assembled products under thermodynamic control; the thermodynamically most favored product is usually obtained due to the dynamic nature of the noncovalent interactions. In this context, it should be challenging to selectively obtain two types of assemblies based only on noncovalent intermolecular interactions. It is essential to use noncovalent interactions that would suppress the interconversion between the two types of assemblies. We expected that relatively

[1]Graduate School of Natural Science and Technology, Kanazawa University, Kakuma-machi, Kanazawa, 920-1192, Japan. [2]Nano Life Science Institute (WPI-NanoLSI), Kanazawa University, Kakuma-machi, Kanazawa, 920-1192, Japan. [3]Present address: Graduate School of Engineering, Nagoya University, Furo-cho, Chikusa-ku, Nagoya, 464-8603, Japan. ✉e-mail: akine@se.kanazawa-u.ac.jp

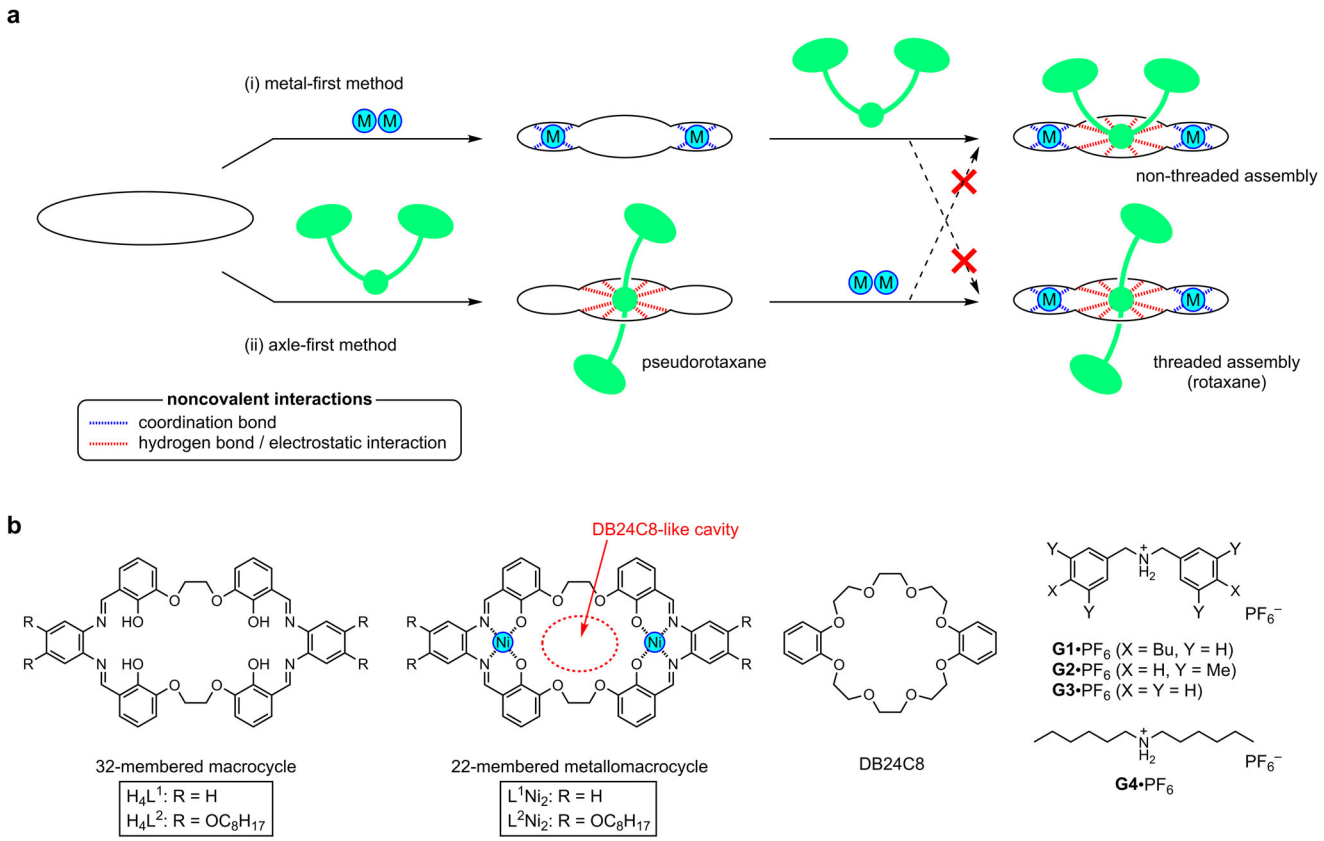

Fig. 1 | Formation of two types of wheel–axle assemblies based only on non-covalent intermolecular interactions. a (i) Metal-first method for non-threaded assembly and (ii) axle-first method for rotaxane-type threaded assembly. **b** Molecular components used in this study, H_4L^1/H_4L^2, L^1Ni_2/L^2Ni_2, DB24C8, and axles (**G1**•PF_6, **G2**•PF_6, **G3**•PF_6, and **G4**•PF_6).

inert coordination bonds can be used in addition to the dynamic hydrogen bonds and electrostatic interactions.

In this study, we successfully obtained two types of wheel–axle assemblies, i.e., the non-threaded and threaded assemblies, based only on the noncovalent interactions (Fig. 1). We focused on a 32-membered macrocycle H_4L^1[1,58] or H_4L^2 as the wheel unit, which shrinks to afford a 22-membered metallomacrocycle upon metalation of the two *N*,*N*′-disalicylidene-*o*-phenylenediamine (H_2saloph) moieties with Ni^{2+}, and a dibenzylammonium derivative as the axle unit, which strongly interacts with large-sized crown ethers. The non-threaded wheel–axle assembly, in which the wheel and axle components are arranged in a face-to-face fashion, was obtained by the metal-first method (Fig. 1a, (i)), i.e., by introduction of Ni^{2+} into the H_4L^2 macrocycle before the complexation with **G1**•PF_6. On the other hand, the rotaxane-type threaded assembly was obtained by the axle-first method (Fig. 1a, (ii)), i.e., by introduction of Ni^{2+} after the formation of a pseudorotaxane from the H_4L^2 wheel and the **G1**•PF_6 axle. Thus, both the non-threaded and threaded wheel–axle assemblies were formed depending on the order of the threading and shrinking steps. (Fig. 1a). We also investigated the different dissociation behaviors of these two types of wheel–axle assemblies upon the addition of Cs^+; only the rotaxane-type threaded assembly remained intact even in the presence of the guest Cs^+.

Results and discussion

Design and synthesis of wheel and axle components

As the wheel unit for the rotaxane structures with dibenzylammonium derivatives, the dibenzo-24-crown-8 (DB24C8) derivatives are known to be the most suitable molecule[59–63]. We expected that the bis(saloph) macrocycle, H_4L^1, in which two H_2saloph units are connected with two O–CH_2CH_2–O linkers, would be a suitable candidate for the wheel component in this study, because its metalated form, L^1Ni_2, has a binding site similar to DB24C8 (Fig. 1b) but shows a significantly higher binding affinity toward cationic species due to the negatively polarized phenoxo groups of the O–Ni–O moieties[64–68]. We have already demonstrated that the H_4L^1 macrocycle shrinks upon metalation due to the formation of two O–Ni–O linkages, and that the resultant DB24C8-like O_8 cavity exhibited an excellent binding affinity to Cs^+[,58]. As the axle component, we expected that the parent dibenzylammonium (**G3**•PF_6) could be used. The unsubstituted benzyl group would act as a sufficiently bulky stopper to prevent the axle from passing through the relatively smaller oval cavity of L^1Ni_2, whereas the flexible DB24C8 is known to require a bulkier stopper such as the 3,5-disubstituted benzyl groups[69–73]. However, these wheel (L^1Ni_2) and axle (**G3**•PF_6) components showed a low solubility in nonpolar solvents, which are essential for strengthening the wheel–axle interaction and increasing the efficiency of the pseudorotaxane formation[59–61]. Therefore, we used their lipophilic analogues, L^2Ni_2 and **G1**•PF_6, which have four peripheral octyloxy groups and two butyl groups, respectively.

The H_4L^2 macrocycle was obtained by the reaction of bis(salicylaldehyde) **1**[58] with an equimolar amount of 4,5-dioctyloxy-1,2-phenylenediamine (**2**)[74] in chloroform/dimethyl sulfoxide (DMSO) at room temperature in 61% yield (Fig. 2a (i)), which basically follows the synthetic procedure of the unsubstituted analogue H_4L^1[1,58]. The formation of the [2 + 2] macrocycle, H_4L^2, was confirmed by the electrospray ionization time-of-flight mass spectrometry (ESI-TOF MS) (m/z = 1261.75 for $[H_4L^2 + H]^+$). The axle **G1**•PF_6 was synthesized via a well-established procedure (Fig. 2b) by the reduction of the imine **3**[75] with $LiAlH_4$ followed by protonation with hydrogen chloride and the subsequent counter anion exchange with ammonium hexafluorophosphate. The axle **G2**•PF_6 containing bulkier stoppers was synthesized according to the literature[76].

As already mentioned, the H_4L^2 macrocycle would shrink to afford the metallomacrocycle, L^2Ni_2, upon the metalation of the H_2saloph

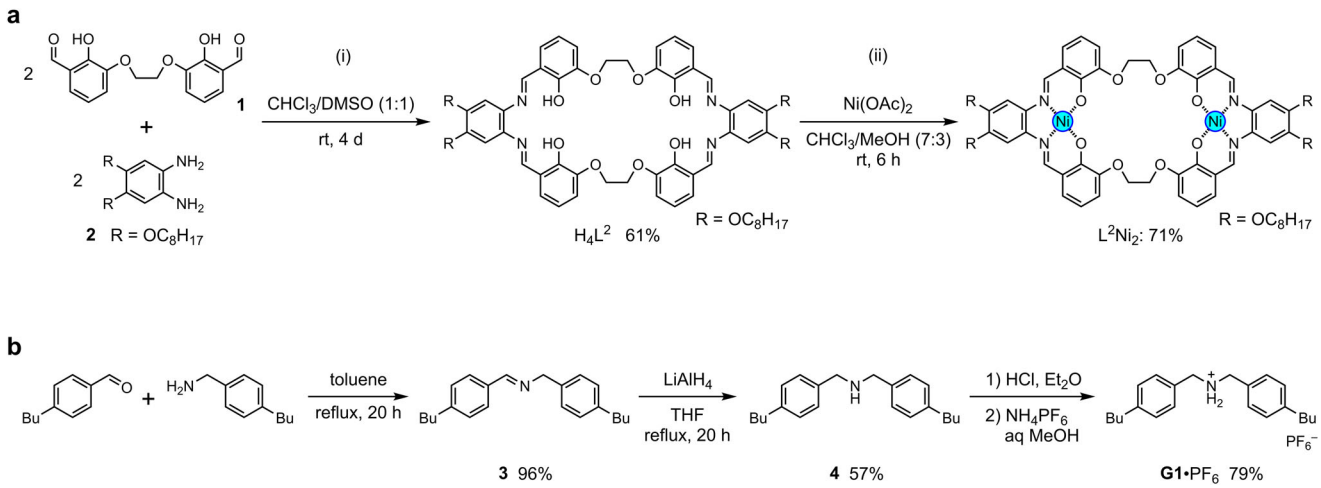

Fig. 2 | Synthetic schemes. a Wheel components (H_4L^2 and L^2Ni_2) and **b** axle component (**G1**•PF_6).

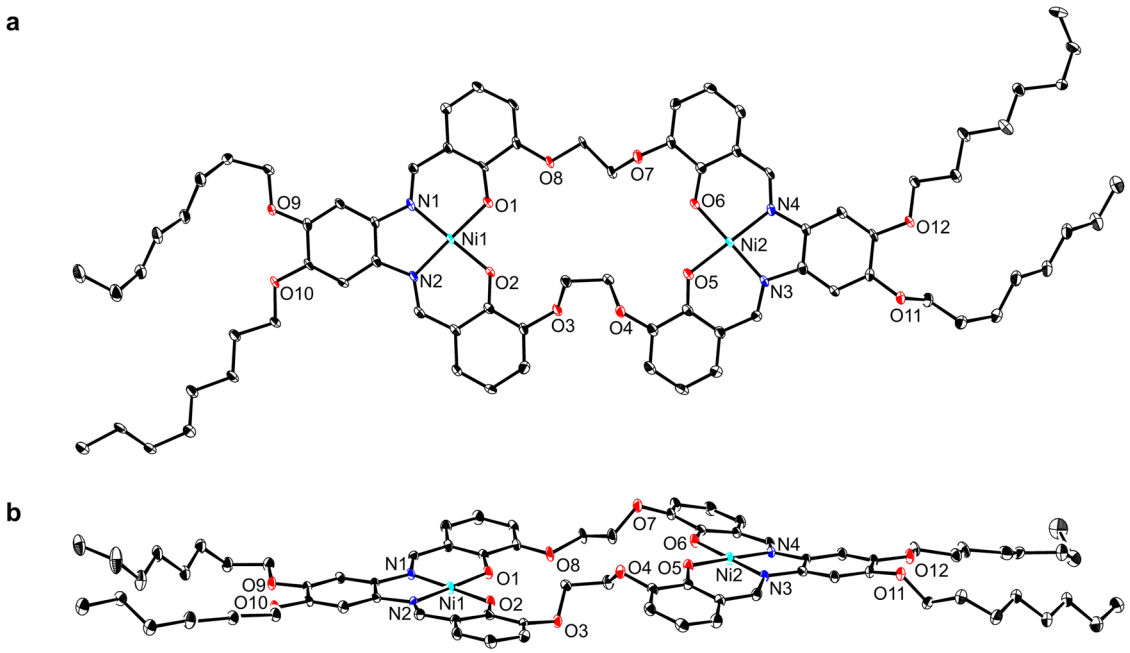

Fig. 3 | X-ray crystal structure of L^2Ni_2 with thermal ellipsoids plotted at the 50% probability level. a top view and **b** side view.

coordination sites. Thus, we investigated the shrinking of the macrocycle in the absence of the axle, which corresponds to the first step of the metal-first method (Fig. 1a (i)). Indeed, the reaction of the H_4L^2 macrocycle with nickel(II) acetate gave the L^2Ni_2 metallomacrocycle in 71% yield (Fig. 2a (ii)), which was characterized by spectroscopic techniques.

The X-ray crystallographic analysis revealed the structure of L^2Ni_2 (Fig. 3), which has a 22-membered macrocyclic structure. The nickel(II) ions have a square planar geometry as observed for the unsubstituted analogue L^1Ni_2[58]. The two [Ni(saloph)] moieties in the L^2Ni_2 macrocycle are situated in an almost coplanar fashion. This relatively planar structure was in sharp contrast to the V-shaped conformation observed for the unsubstituted analogue L^1Ni_2 in the crystalline state[58]. Since introduction of the peripheral alkyl/alkoxy groups does not usually have a significant influence on the most stable conformation in solution, this structural diversity implies the sufficient flexibility of the L^2Ni_2 wheel, which allows adoption of various conformations from the planar to the V-shaped structures in solution.

Formation of non-threaded wheel–axle assembly

We then investigated the formation of the wheel–axle assembly according to the metal-first method (Fig. 1a (i)) using the pre-formed L^2Ni_2 as the synthetic intermediate. The interaction of the wheel L^2Ni_2 with the axle **G1**•PF_6 was clearly demonstrated by the ^{1}H nuclear magnetic resonance (NMR) titration experiments in $CDCl_3/CD_3CN$ (4:1). The addition of **G1**•PF_6 to L^2Ni_2 caused significant chemical shift changes indicative of the strong wheel–axle interaction (Fig. 4a (i)–(iv)). The binding constant for the 1:1 complexation was determined to be $\log K_a = 4.0 \pm 0.2$ by a nonlinear least-squares regression (Supplementary Fig. S1).

In the ^{1}H NMR titration experiment, the wheel–axle assembly was observed at the chemical shifts that are averaged with the wheel or axle component; for example, only one set of signals for the L^2Ni_2 macrocycle was observed when 0.5 equiv of **G1**•PF_6 was present. This suggests the fast exchange kinetics for the formation/dissociation equilibrium of this wheel–axle assembly on the ^{1}H NMR time scale. This observation is in contrast to the behavior observed for the interaction of the fully organic DB24C8 wheel with the same axle **G1**•PF_6, which showed signals for the pseudorotaxane DB24C8•**G1**•PF_6 separate from each of the axle and wheel

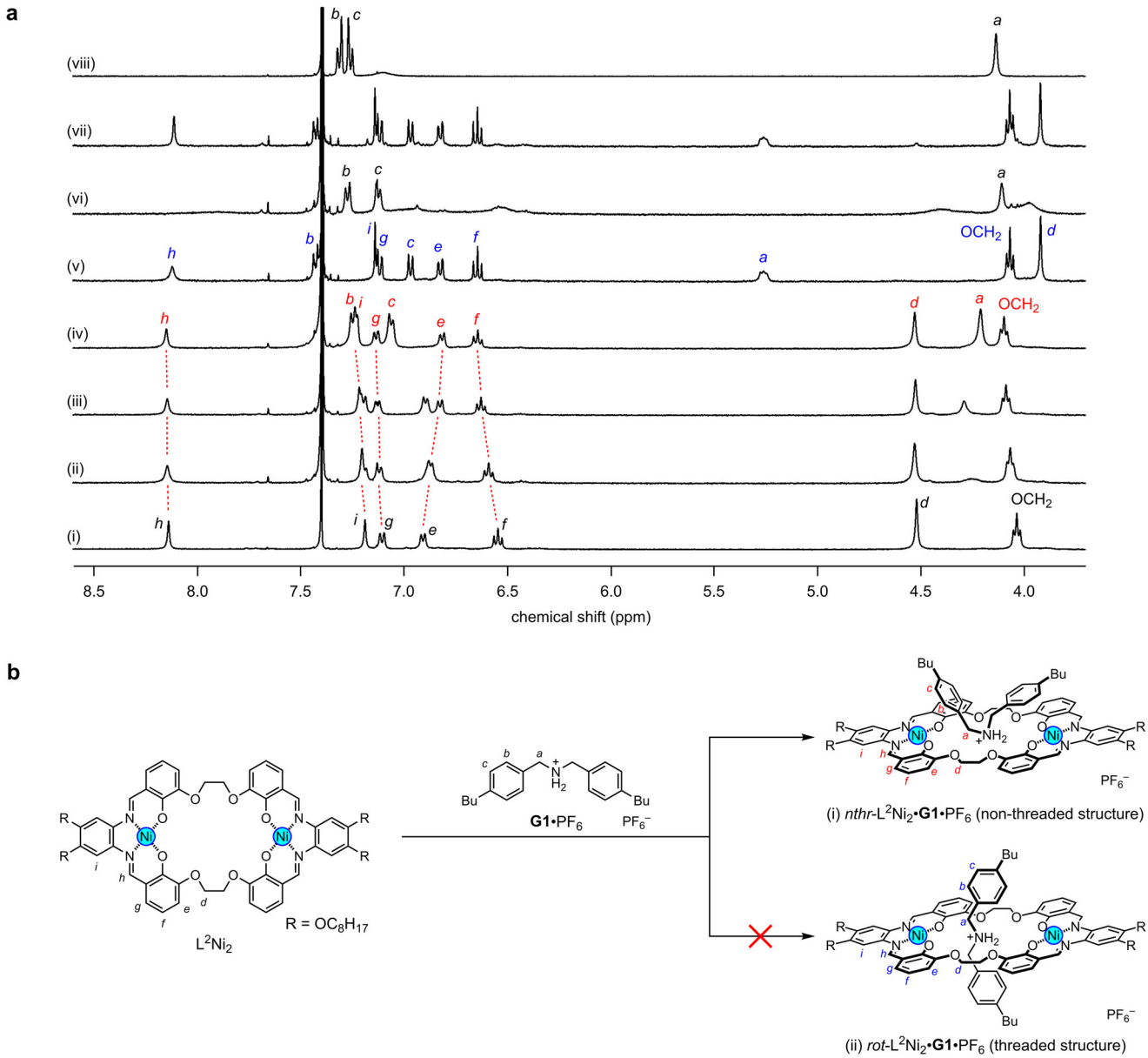

Fig. 4 | Interaction of L^2Ni_2 metallomacrocycle with the G1•PF_6 axle. a ^{1}H NMR spectra of non-threaded and threaded wheel–axle assemblies of L^2Ni_2 and **G1**•PF_6 (400 MHz, $CDCl_3/CD_3CN$ (4:1)). (i–iv) Spectral changes of L^2Ni_2 upon the addition of **G1**•PF_6 (i, 0 equiv, ii, 0.5 equiv, iii, 1.0 equiv, iv, 2.0 equiv) indicative of the formation of the non-threaded assembly, *nthr*-L^2Ni_2•**G1**•PF_6; (v) isolated rotaxane-type threaded assembly, *rot*-L^2Ni_2•**G1**•PF_6; (vi) *nthr*-L^2Ni_2•**G1**•PF_6 in the presence of CsOTf (2 equiv); (vii) *rot*-L^2Ni_2•**G1**•PF_6 in the presence of CsOTf (2 equiv); (viii) uncomplexed **G1**•PF_6. **b** Formation of *nthr*-L^2Ni_2•**G1**•PF_6 from L^2Ni_2 and **G1**•PF_6 (metal-first method). The ^{1}H NMR signal assignments of *nthr*- and *rot*-L^2Ni_2•**G1**•PF_6 are also shown.

components (Supplementary Fig. S2). This independently observed set of signals including the downfield shifted axle benzyl proton (4.56 ppm) is an indication of the rotaxane-type threaded structure[59–63]. The spectral changes for the L^2Ni_2–**G1**•PF_6 complexation without emergence of the separate set of signals are rather similar to those observed for the DB24C8–**G2**•PF_6 titration experiments showing only slight changes in the chemical shifts (Supplementary Fig. S3); in this case, the 3,5-dimethylbenzyl groups in the axle **G2**•PF_6 are too large to be threaded/dethreaded into the DB24C8 macrocycle[70–73].

Based on these experimental results, it is reasonable to conclude that the L^2Ni_2 wheel and the **G1**•PF_6 axle form a loosely-bound non-threaded wheel–axle assembly[77–81] (Fig. 1a (i)), i.e., *nthr*-L^2Ni_2•**G1**•PF_6 (Fig. 4b (i)), in which the association/dissociation processes are fast on the ^{1}H NMR time scale, rather than the rotaxane-type threaded assembly, *rot*-L^2Ni_2•**G1**•PF_6 (Fig. 4b (ii)). The loose character of the non-threaded wheel–axle assembly, *nthr*-L^2Ni_2•**G1**•PF_6, was consistent with the mass spectrometric observation, which mainly showed the dissociated species, whereas the corresponding rotaxane-type threaded assembly only exhibited the bound species under the same conditions (see below). Nevertheless, the wheel–axle interaction for the *nthr*-L^2Ni_2•**G1**•PF_6 assembly ($\log K_a = 4.0$) was approximately two orders of magnitude stronger than that for the DB24C8•**G2**•PF_6 ($\log K_a = 2.37$ Supplementary Fig. S3), which makes the non-threaded assembly *nthr*-L^2Ni_2•**G1**•PF_6 more clearly observable than the crown ether analogues showing very small chemical shift changes. The formation efficiency was presumably enhanced by the negatively polarized phenoxo groups of the [Ni(saloph)] moieties in L^2Ni_2.

Formation of rotaxane-type threaded wheel-axle assembly

As already described, the wheel–axle assembly obtained by mixing the L^2Ni_2 and **G1**•PF_6 does not have a rotaxane-type threaded structure but a non-

threaded structure (Fig. 4b). This means that either the *p*-substituted benzyl group in the axle **G1**•PF_6 is sufficiently large with respect to the small oval cavity of the L^2Ni_2 macrocycle to prevent the rotaxane formation or this is just because the non-threaded assembly is more thermodynamically stable than the rotaxane-type threaded assembly. Thus, we attempted the synthesis of the rotaxane according to the axle-first method (Fig. 1a (ii)), i.e., the metalation-driven shrinking strategy[54] starting from the non-metalated H_4L^2 macrocycle and **G1**•PF_6 axle.

In fact, in order to obtain the targeted rotaxane according to the axle-first method, the pseudorotaxane intermediate between H_4L^2 and **G1**•PF_6 should be efficiently formed before the metalation-driven shrinking. As expected, the pseudorotaxane was almost quantitatively formed simply by mixing the two components (Fig. 5a (i)). The ^{1}H NMR titration experiment exhibited signals of the pseudorotaxane separately from those of its constituents, H_4L^2 and **G1**•PF_6 (Supplementary Fig. S4), which is indicative of the rotaxane-type threaded structure of H_4L^2•**G1**•PF_6 with a slow formation/dissociation equilibrium. The axle benzyl proton H_a was significantly downfield shifted (from 4.13 ppm to 4.68 ppm) upon complexation, which could be attributed to the strong C–H···O interactions with the oxygen atoms in the H_4L^2 macrocycle, and the wheel–axle ROE correlations agreed with the rotaxane-type

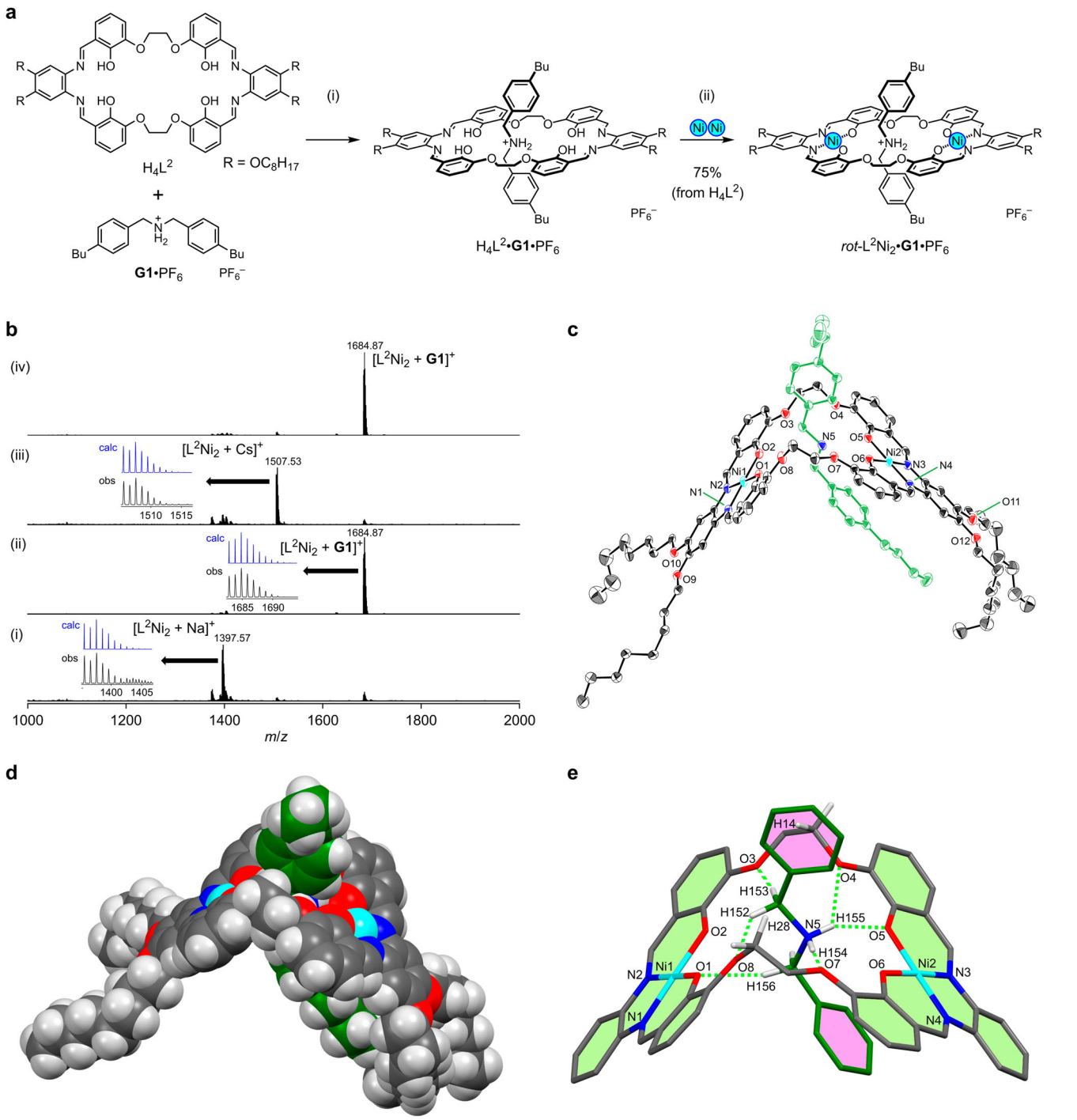

Fig. 5 | Formation and characterization of rotaxane-type threaded wheel–axle assembly. a Formation of *rot*-L^2Ni_2•**G1**•PF_6 by metalation of the pseudorotaxane H_4L^2•**G1**•PF_6 (axle-first method). **b** ESI-TOF mass spectra of (i) *nthr*-L^2Ni_2•**G1**•PF_6, (ii) *rot*-L^2Ni_2•**G1**•PF_6, (iii) *nthr*-L^2Ni_2•**G1**•PF_6 + CsOTf (2 equiv), and (iv) *rot*-L^2Ni_2•**G1**•PF_6 + CsOTf (2 equiv). **c**–**e** X-ray crystal structure of *rot*-L^2Ni_2•**G1**•PF_6 (only one of the crystallographically independent molecules is shown). **c** Thermal ellipsoid plot (15% probability level), **d** space-filling model, and **e** capped stick model with peripheral groups omitted to show N–H···O and C–H···O interactions.

threaded structure (Supplementary Fig. S5). The tightly-bound structure was evidenced by the mass spectrometric measurement ($m/z = 1572.00$ for $[H_4L^2 + \mathbf{G1}]^+$; Supplementary Fig. S6). It is noteworthy that 1 equiv of **G1**•PF_6 was sufficient for the complete conversion of H_4L^2 to this pseudorotaxane, indicating the very strong wheel–axle binding. Therefore, this pseudorotaxane, H_4L^2•**G1**•PF_6, would be a suitable precursor for the rotaxane-type threaded wheel–axle assembly by mechanically interlocking based on the shrinking strategy (axle-first method; Fig. 1a (ii)).

We then investigated the introduction of Ni^{2+} into the coordination sites of the H_4L^2 macrocycle while keeping the threaded structure of the pseudorotaxane, H_4L^2•**G1**•PF_6. As expected, this conversion quite efficiently proceeded to give the targeted rotaxane, *rot*-L^2Ni_2•**G1**•PF_6, in 75% isolated yield simply by the reaction with nickel(II) acetate (Fig. 5a (ii)). The ^{1}H NMR spectrum of the product no longer showed the phenolic OH signal, confirming the metalation of the H_2saloph coordination sites. The axle benzyl proton H_a was observed in the downfield shifted region (5.25 ppm), which is consistent with the threaded rotaxane structure (Fig. 4a (v)). The wheel–axle ROE correlations also support the threaded structure (Supplementary Fig. S7).

It should be noted that the ^{1}H NMR spectrum of this *rot*-L^2Ni_2•**G1**•PF_6 was completely different from that of the non-threaded wheel–axle assembly, *nthr*-L^2Ni_2•**G1**•PF_6, which was formed simply by mixing the L^2Ni_2 wheel and the **G1**•PF_6 axle (Fig. 4a (iv, v)). The ESI-TOF mass spectrum was also supportive of the firmly-interlocked structure, showing the $[L^2Ni_2 + \mathbf{G1}]^+$ assembly as an intense peak at $m/z = 1684.87$ without showing the dissociated species (Fig. 5b (ii)). This is in contrast to the mass spectrum of the non-threaded assembly, *nthr*-L^2Ni_2•**G1**•PF_6, which predominantly showed the dissociated species at $m/z = 1397.57$ $[L^2Ni_2 + Na]^+$ (Fig. 5b (i)). These mass spectrometric investigations are in good agreement with the rotaxane-type threaded structure of *rot*-L^2Ni_2•**G1**•PF_6, which is not in equilibrium with the non-threaded assembly, *nthr*-L^2Ni_2•**G1**•PF_6.

The rotaxane-type threaded structure was unambiguously confirmed by X-ray crystallography (Fig. 5c). The crystal contains two crystallographically independent assemblies of *rot*-L^2Ni_2•**G1**•PF_6 with a similar conformation, in which the $\mathbf{G1}^+$ axle is threaded into the L^2Ni_2 wheel (Supplementary Fig. S8). The space-filling representation of the molecular structure clearly showed the bulkiness of the *p*-butylbenzyl stopper groups with respect to the L^2Ni_2 cavity (Fig. 5d), enabling the isolation of the interlocked rotaxane species. The two interlocked entities, L^2Ni_2 and $\mathbf{G1}^+$, are noncovalently bound through the N–H···O, C–H···O, C–H···π, and π-stacking interactions (Fig. 5e). Unlike the relatively planar conformation of the uncomplexed L^2Ni_2 wheel in the crystalline state (Fig. 3), the L^2Ni_2 wheel in the rotaxane structure adopted a V-shaped bent conformation with the dihedral angle of 84.1° or 106.1° between the two [Ni(saloph)] units.

As already described, the non-threaded wheel–axle assembly was formed by the metal-first method (Fig. 1a (i)), i.e., simply by mixing the pre-metalated L^2Ni_2 macrocycle with the **G1**•PF_6 axle in solution, while the rotaxane-type threaded assembly was formed by the axle-first method (Fig. 1a (ii)), i.e., by the metal-induced shrinking of the pre-formed H_4L^2•**G1**•PF_6 pseudorotaxane. Thus, two kinds of wheel–axle assemblies, non-threaded and threaded, were selectively formed by changing the order of addition of the metal and axle, even though both the metal and axle are bound via noncovalent interactions.

We found that the phenyl groups in the axle **G1**•PF_6 were essential to obtain the rotaxane-type threaded assembly based on the following experiments using the less bulky axle, **G4**•PF_6, without a phenyl group. When **G4**•PF_6 was mixed with the L^2Ni_2 macrocycle according to the metal-first method, chemical shift changes were observed in the ^{1}H NMR spectra, suggesting an interaction between the two species with a fast association/dissociation equilibrium (Supplementary Fig. S9). The signal of the NH_2–CH_2 group did not show the downfield shift indicative of the threaded structure. This suggested that the non-threaded assembly, *nthr*-L^2Ni_2•**G4**•PF_6, is dominating in the mixture. The axle-first method was also employed as an alternative method, but only the unreacted L^2Ni_2 macrocycle was recovered without producing the rotaxane. These results suggested that the threaded assembly, *rot*-L^2Ni_2•**G4**•PF_6, readily undergoes dethreading, because it is less stable than the non-threaded assembly, *nthr*-L^2Ni_2•**G4**•PF_6, and it has no phenyl groups as the stopper. Therefore, the phenyl groups of the axle **G1**•PF_6 are essential for the formation of the rotaxane-type threaded assembly.

Computational studies of the wheel–axle assemblies

The structures and stabilities of the non-threaded and threaded wheel–axle assemblies were investigated by density functional theory (DFT) calculations for the unsubstituted analogue L^1Ni_2•$\mathbf{G3}^+$ for simplicity (Fig. 6; Supplementary Figs. S10 and S11). For the two types of assemblies, several different conformations were optimized in order to find the global-minimum structures, and the interaction energies were evaluated by the supermolecule method taking into account the counterpoise basis set superposition error (BSSE) correction.

The most stable structure of the non-threaded assembly, *nthr-a*-L^1Ni_2•$\mathbf{G3}^+$, contains the $\mathbf{G3}^+$ axle with a folded conformation, which was located inside the cleft of the V-shaped L^1Ni_2 wheel (Fig. 6a). The four protons of the NH_2–CH_2 moiety in the $\mathbf{G3}^+$ axle effectively interacted with the L^1Ni_2 oxygen atoms through the N–H···O and C–H···O hydrogen bonds. The L^1Ni_2 macrocycle adopted a twisted V-shaped conformation, and six out of their eight oxygen atoms participated in the hydrogen bonds. In addition, one of the benzene rings of the $\mathbf{G3}^+$ axle was stacked on top of the square planar nickel(II) at a distance of 3.2–3.3 Å. These noncovalent interactions probably contributed to the strong association between the L^1Ni_2 and $\mathbf{G3}^+$ components even though they did not form a threaded structure.

For the rotaxane-type threaded assemblies, we obtained two different stable structures within 2 kJ mol^{-1}, *rot-a*- and *rot-b*-L^1Ni_2•$\mathbf{G3}^+$, which have

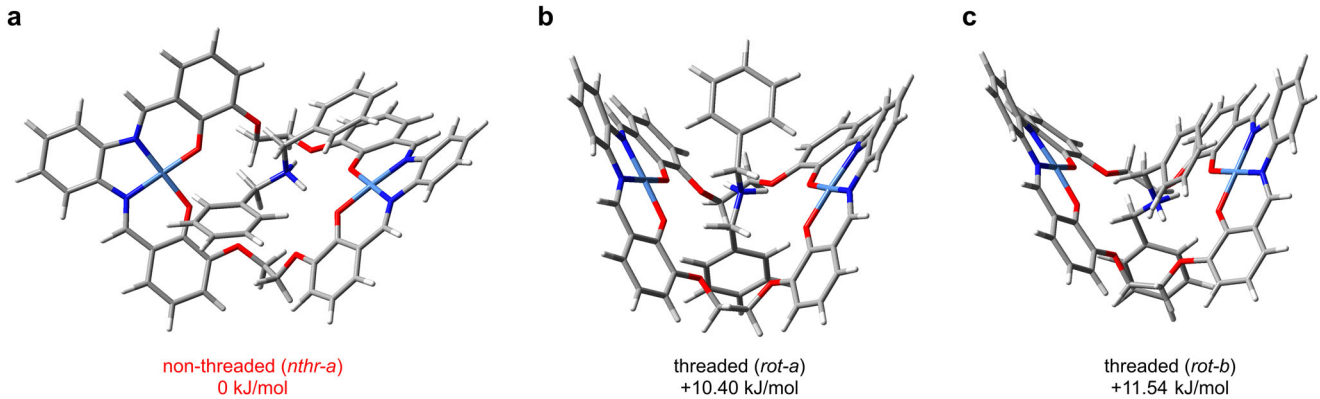

Fig. 6 | Optimized structures of the wheel–axle assemblies. a *nthr-a*-L^1Ni_2•$\mathbf{G3}^+$, **b** *rot-a*-L^1Ni_2•$\mathbf{G3}^+$, and **c** *rot-b*-L^1Ni_2•$\mathbf{G3}^+$ (DFT, wB97XD, 6-31 G(d,p)).

the **G3**$^+$ axle in different orientations (Fig. 6b, c). The *rot-a*-L^{1}Ni$_2$•**G3**$^+$ is the global-minimum structure, and the second stable *rot-b*-L^{1}Ni$_2$•**G3**$^+$ has a conformation similar to the X-ray crystal structure of *rot*-L^{2}Ni$_2$•**G1**•PF$_6$. Both structures have the L^{1}Ni$_2$ macrocycle with a V-shaped conformation, in which the four protons of the NH_2–CH_2 moiety were hydrogen bonded to the L^{1}Ni$_2$ oxygen atoms. Unlike the non-threaded structure, all the eight oxygen atoms in the L^{1}Ni$_2$ macrocycle participated in the hydrogen bonds to the **G3**$^+$ axle with the H···O distances in the range of 1.8–2.5 Å.

These threaded assemblies, *rot-a-* and *rot-b*-L^{1}Ni$_2$•**G3**$^+$, are approximately 10 kJ mol^{-1} less stable than the non-threaded assembly, *nthr-a*-L^{1}Ni$_2$•**G3**$^+$ (Table 1). The formation energies E_{form} for *rot-a-* and *rot-b*-L^{1}Ni$_2$•**G3**$^+$ are also 10 kJ mol^{-1} smaller than that for *nthr-a*-L^{1}Ni$_2$•**G3**$^+$, because these two types of assemblies consist of the same wheel and axle constituents. In contrast, the interaction energy E_{int} between the two constituents, which was estimated by the supermolecule method, showed a different trend. The wheel–axle interactions of *nthr-a*-L^{1}Ni$_2$•**G3**$^+$ and *rot-a*-L^{1}Ni$_2$•**G3**$^+$ are similar, but that of *rot-b*-L^{1}Ni$_2$•**G3**$^+$ is significantly stronger by more than 20 kJ mol^{-1}.

The stability difference between the non-threaded and threaded assemblies of L^{1}Ni$_2$•**G3**$^+$ can be reasonably explained by the strain energies of each constituent, $E_{def(W)}$ and $E_{def(A)}$ (Table 1). In particular, the strain energies for the wheel component of *rot-a-* and *rot-b*-L^{1}Ni$_2$•**G3**$^+$ are more than 80 kJ mol^{-1}, which are 22–25 kJ mol^{-1} higher than that of *nthr-a*-L^{1}Ni$_2$•**G3**$^+$. Thus, the intercomponent interaction between the L^{1}Ni$_2$ wheel and the **G3**$^+$ axle can be maximized in the threaded structure, but this is energetically less favorable mainly because its elliptical cavity needs to deform to accommodate the **G3**$^+$ axle, leading to the increased strain energies.

Table 1 | Stability of L^{1}Ni$_2$•G3$^+$ assemblies estimated by DFT calculations (energies in kJ mol^{-1})

	E_{rel} [a]	E_{form} [b]	E_{int} [c]	$E_{def(W)}$ [d]	$E_{def(A)}$ [d]
nthr-a-L^{1}Ni$_2$•**G3**$^+$	0	–322.98	–364.12	59.99	19.63
rot-a-L^{1}Ni$_2$•**G3**$^+$	+10.40	–312.58	–365.71	81.81	14.31
rot-b-L^{1}Ni$_2$•**G3**$^+$	+11.54	–311.44	–385.87	85.07	26.33

[a] E_{rel}: relative stability with respect to *nthr-a*-L^{1}Ni$_2$•**G3**$^+$. [b] $E_{form} = E_{WA} - E_W - E_A$, where E_{WA}, E_W, and E_A are the energies of the optimized structures of the assembly (WA), wheel (W), and axle (A), respectively. [c] E_{int} is the BSSE-corrected interaction energies determined by the supermolecule method. [d] $E_{def(W)}$ and $E_{def(A)}$: energy increase of the wheel (W) and axle (A) molecules by the geometrical deformation associated with the formation of the assemblies.

As suggested by the computational investigations, the experimentally obtained non-threaded assembly, *nthr*-L^{2}Ni$_2$•**G1**•PF$_6$, should be energetically more favorable than the threaded assembly, *rot*-L^{2}Ni$_2$•**G1**•PF$_6$. Before the metalation of the macrocycle H_4L^2, however, the threaded assembly, pseudorotaxane H_4L^2•**G1**•PF$_6$, was spontaneously formed simply by mixing the H_4L^2 and **G1**•PF$_6$ (Fig. 5a). Obviously, the introduction of nickel(II) ions destabilizes the threaded structure, resulting in the reversed relative stability of the non-threaded and threaded assemblies. At the same time, this metalation suppresses the interconversion between the non-threaded and threaded assemblies by making the macrocycle smaller so that it does not allow the phenyl groups to pass through. This is consistent with the observation that the rotaxane-type threaded assembly was kinetically trapped only when phenyl substituted **G1**•PF$_6$ was used as the axle component while the dialkylammonium axle **G4**•PF$_6$ did not give the rotaxane structure.

Dissociation of the non-threaded assembly by Cs$^+$

We have previously reported that the unsubstituted L^{1}Ni$_2$ macrocycle showed a strong binding affinity to Cs$^+$ even in a polar solvent that could diminish the electrostatic interactions (logK_a = 4.94 in DMSO-d_6)[58]. This interaction with Cs$^+$ could be sufficiently strong to replace the **G1**$^+$ axle to demonstrate the labile nature of the non-threaded *nthr*-L^{2}Ni$_2$•**G1**•PF$_6$ assembly, but not to replace if the **G1**$^+$ axle was mechanically interlocked in the rotaxane-type threaded assembly, *rot*-L^{2}Ni$_2$•**G1**•PF$_6$.

When CsOTf was added to the non-threaded assembly, *nthr*-L^{2}Ni$_2$•**G1**•PF$_6$, the ^{1}H NMR spectra showed significant changes in the chemical shifts, which are indicative of the interaction with Cs$^+$(Fig. 4a (vi)). The ESI-TOF mass spectrum of the mixture showed the peak at *m/z* = 1507.53 assignable to [L^{2}Ni$_2$ + Cs]$^+$ without showing intense peaks for the wheel–axle assembly (Fig. 5b (iii)). Therefore, Cs$^+$ almost completely replaced the **G1**$^+$ axle of the non-threaded wheel–axle assembly, *nthr*-L^{2}Ni$_2$•**G1**•PF$_6$ (Fig. 7 (i)). In contrast, the addition of CsOTf to the rotaxane-type threaded wheel–axle assembly, *rot*-L^{2}Ni$_2$•**G1**•PF$_6$, caused no change in the ^{1}H NMR and ESI-TOF mass spectra (Figs. 4a (vii) and 5b (iv)). These results indicated that the **G1**$^+$ axle in the rotaxane was firmly interlocked with the L^{2}Ni$_2$ macrocycle even in the presence of the Cs$^+$ that could more strongly interact with the L^{2}Ni$_2$ macrocycle (Fig. 7 (ii)). This confirms the kinetic stability of the rotaxane-type threaded assembly, *rot*-L^{2}Ni$_2$•**G1**•PF$_6$, which is maintained only by coordination bonds used for the shrinking step in the axle-first method.

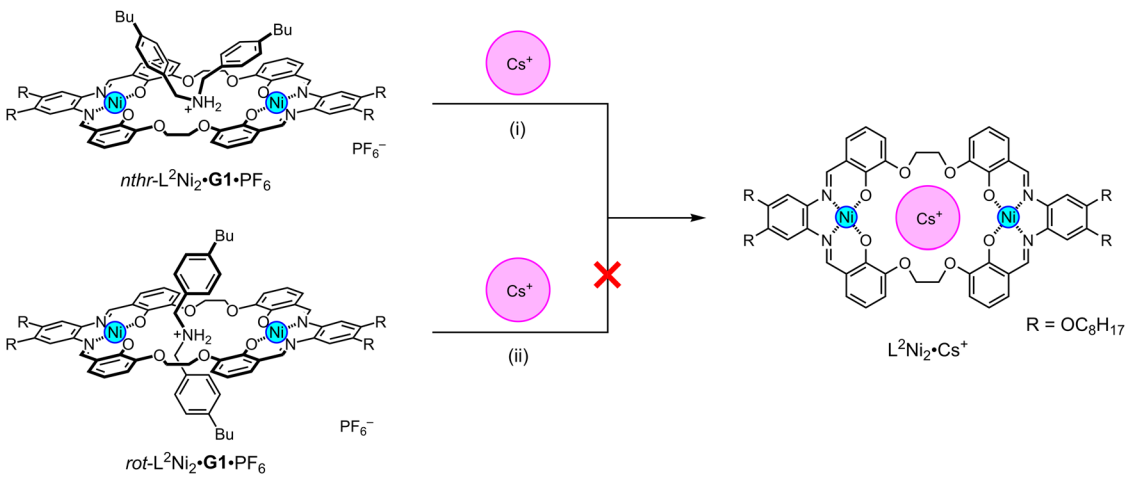

Fig. 7 | Reactions of two types of wheel–axle assemblies with Cs$^+$. (i) The non-threaded assembly, *nthr*-L^{2}Ni$_2$•**G1**•PF$_6$, readily dissociates into its components to give L^{2}Ni$_2$•Cs$^+$; (ii) The rotaxane-type threaded assembly, *rot*-L^{2}Ni$_2$•**G1**•PF$_6$, remains intact in the presence of Cs$^+$.

Conclusions

In conclusion, we have selectively obtained two kinds of wheel–axle assemblies, the non-threaded assembly (*nthr*-L^2Ni_2•**G1**•PF_6) and the rotaxane-type threaded assembly (*rot*-L^2Ni_2•**G1**•PF_6), simply by changing the order of the wheel–axle complexation and the metal-induced shrinking of the H_4L^2 macrocycle. The complexation of the pre-formed L^2Ni_2 wheel with the **G1**•PF_6 axle (metal-first method) resulted in the formation of a non-threaded assembly (*nthr*-L^2Ni_2•**G1**•PF_6), which can easily dissociate to give L^2Ni_2•Cs^+ by the addition of Cs^+. The formation efficiency of the non-threaded assembly was presumably enhanced by the negatively polarized phenoxo groups of the [Ni(saloph)] moieties in L^2Ni_2. On the other hand, the rotaxane-type threaded assembly (*rot*-L^2Ni_2•**G1**•PF_6) was efficiently obtained by the metal-induced shrinking of the pre-formed pseudorotaxane, H_4L^2•**G1**•PF_6 (axle-first method). This threaded assembly did not dissociate into its constituents even in the presence of Cs^+, confirming the firmly interlocked nature of the rotaxane-type threaded assembly, *rot*-L^2Ni_2•**G1**•PF_6.

In general, coordination bonds are categorized as noncovalent interactions that provide reversibility in the supramolecular self-assembling processes[82,83]. In fact, several metal-containing rotaxanes whose interlocked structure is maintained only by coordination bonds[32–53] showed a sufficient dynamic feature that affords the thermodynamically most stable structure due to the equilibration. In this study, thanks to this dynamic feature, we can easily change the order of the wheel–axle complexation and the metal-induced shrinking to obtain two different kinds of wheel–axle assemblies. Nevertheless, both of these isomeric assemblies can be obtained due to the relatively inert nature of the Ni–N and Ni–O coordination bonds used for the shrinking step. It is well known that the dynamic nature of coordination bonds can be easily tuned by changing the external and environmental factors, e.g., solvents, additives, and redox reactions, which could facilitate switching between the two types of wheel–axle assemblies and enabling/disabling the interconversions between them. Further studies of the stimuli-responsive structural conversions of dynamic metallorotaxanes are currently underway.

Methods

Materials and methods

The reagents and solvents were purchased from Fujifilm Wako Pure Chemical or TCI and used without further purification. The ^{1}H NMR spectra were recorded on a JEOL JNM-ECS 400 (400 MHz), a Bruker Avance Neo 400 (400 MHz), or a Bruker Avance Neo 600 (600 MHz). The ^{13}C NMR spectra were recorded on a JEOL JNM-ECS 400 (100 MHz) or a Bruker Avance Neo 600 (150 MHz). Chemical shifts were referenced with respect to tetramethylsilane (0 ppm for ^{1}H and ^{13}C) as an internal standard or the solvent residual peaks. The ESI-TOF mass spectra were recorded on a Bruker Daltonics micrOTOF II. The synthetic precursors, bis(salicylaldehyde) **1**[58], 4,5-dioctyloxy-1,2-phenylenediamine (**2**)[74], and ammonium salt **G2**•PF_6[76] were prepared according to the literature. The ^{1}H and ^{13}C NMR spectra of new compounds were shown in Supplementary Information (Supplementary Figs. S12–S21).

Synthesis of 3

A solution containing 4-butylbenzylamine[84] (483 mg, 2.96 mmol) and 4-butylbenzaldehyde (486 mg, 2.98 mmol) in dehydrated toluene (6 mL) was heated to reflux for 20 h. After cooling to room temperature, the mixture was concentrated to dryness to give the imine **3**[75] (875 mg, 2.85 mmol, 96%) as a yellow oil. ^{1}H NMR (400 MHz, $CDCl_3$): δ 8.34 (s, 1H), 7.68 (d, J = 8.0 Hz, 2H), 7.22 (d, J = 8.0 Hz, 2H), 7.21 (d, J = 8.0 Hz, 2H), 7.14 (d, J = 8.0 Hz, 2H), 4.77 (s, 2H), 2.63 (t, J = 7.7 Hz, 2H), 2.57 (t, J = 7.7 Hz, 2H), 1.60 (quint, J = 7.7 Hz, 2H), 1.58 (quint, J = 7.6 Hz, 2H), 1.35 (sext, J = 7.4 Hz, 2H), 1.34 (sext, J = 7.4 Hz, 2H), 0.92 (t, J = 7.3 Hz, 3H), 0.91 (t, J = 7.3 Hz, 3H); ^{13}C NMR (100 MHz, $CDCl_3$): δ 161.76, 145.97, 141.54, 136.51, 133.75, 128.64, 128.48, 128.23, 127.87, 64.82, 35.61, 35.31, 33.70, 33.42, 22.34, 22.32, 13.95, 13.92 (Supplementary Data 1,2).

Synthesis of 4

Under a nitrogen atmosphere, a solution of the imine **3** (1.52 g, 4.93 mmol) in THF (15 mL) was added dropwise to a suspension of lithium aluminum hydride (1.38 g, 36.4 mmol) in THF (20 mL) at 0 °C and the mixture was heated to reflux for 20 h. After cooling to room temperature, the reaction mixture was quenched with an aqueous sodium sulfate solution. The resultant solid was filtered off and the filtrate was extracted with diethyl ether. The organic layer was washed with water, then brine, dried over anhydrous magnesium sulfate, filtered, and concentrated to dryness to obtain **4** (870 mg, 2.81 mmol, 57%) as a colorless oil. ^{1}H NMR (400 MHz, $CDCl_3$): δ 7.23 (d, J = 8.0 Hz, 4H), 7.13 (d, J = 8.0 Hz, 4H), 3.77 (s, 4H), 2.59 (t, J = 7.7 Hz, 4H), 1.6 (br), 1.59 (quint, J = 7.6 Hz, 4H), 1.35 (sext, J = 7.4 Hz, 4H), 0.92 (t, J = 7.3 Hz, 6H); ^{13}C NMR (100 MHz, $CDCl_3$): δ 141.52, 137.46, 128.39, 128.04, 52.93, 35.31, 33.71, 22.37, 13.96 (Supplementary Data 3,4).

Synthesis of G1•PF_6

Hydrogen chloride gas, which was generated by N_2 bubbling into concentrated hydrochloric acid, was bubbled into a solution of the amine **4** (349 mg, 1.13 mmol) in diethyl ether (12 mL) for 5 min. The white precipitates of **G1**•Cl were collected by filtration. This **G1**•Cl was dissolved in methanol (8 mL), then an aqueous solution of ammonium hexafluorophosphate (9.13 g, 56.0 mmol in 35 mL) was added. The resultant white precipitates were collected by filtration, thoroughly washed with water, and dried in vacuo to obtain **G1**•PF_6 (406 mg, 0.89 mmol, 79%) as colorless crystals. ^{1}H NMR (400 MHz, $CDCl_3$) δ 10.09 (br, 2H), 7.39 (d, J = 8.0 Hz, 4H), 7.16 (d, J = 8.0 Hz, 4H), 3.79 (s, 4H), 2.52 (t, J = 7.8 Hz, 4H), 1.50 (quint, J = 7.6 Hz, 4H), 1.30 (sext, J = 7.4 Hz, 4H), 0.88 (t, J = 7.3 Hz, 6H); ^{13}C NMR (100 MHz, $CDCl_3$) δ 145.34, 129.70, 129.62, 126.11, 50.64, 35.32, 33.27, 22.32, 13.89; ESI-MS (m/z): [**G1**]$^+$ calcd. for $C_{22}H_{32}N$, 310.2535; found, 310.2552 (Supplementary Data 5,6).

Synthesis of H_4L^2

Under a nitrogen atmosphere, a solution of 4,5-dioctyloxy-1,2-phenylenediamine (**2**) (21 mM in dehydrated chloroform, 10 mL, 0.21 mmol) was added to a solution of the bis(salicylaldehyde) **1** (60.0 mg, 0.198 mmol) in dry DMSO (10 mL). The reaction mixture was left to stand at room temperature for 4 d. The reaction mixture was then filtered and concentrated to a minimal volume. The residue was poured into water and extracted with chloroform (50 mL × 3). The combined organic extract was washed with water (50 mL × 2), dried over anhydrous sodium sulfate, filtered, and concentrated to dryness. The crude product was purified by reprecipitation from chloroform/hexane followed by centrifugation (three times) of the methanol suspension to yield H_4L^2 (76.6 mg, 60.7 μmol, 61%) as yellow crystals. ^{1}H NMR (600 MHz, $CDCl_3$): δ 13.42 (s, 4H), 8.60 (s, 4H), 7.20 (dd, J = 7.8, 1.1 Hz, 4H), 7.07 (dd, J = 7.8, 1.1 Hz, 4H), 6.83 (t, J = 7.8 Hz, 4H), 6.83 (s, 4H), 4.43 (s, 8H), 4.07 (t, J = 6.6 Hz, 8H), 1.86 (quint, J = 7.3 Hz, 8H), 1.51 (quint, J = 7.3 Hz, 8H), 1.40–1.25 (m, 32H), 0.89 (t, J = 6.9 Hz, 12H); ^{13}C NMR (150 MHz, $CDCl_3$): δ 162.08, 153.05, 149.04, 147.45, 135.29, 125.78, 121.91, 120.05, 118.57, 105.08, 70.02, 69.84, 31.84, 29.39, 29.29 (×2), 26.05, 22.68, 14.11; HRMS (ESI-TOF) (m/z): [H_4L^2 + H]$^+$ calcd. for $C_{76}H_{100}N_4O_{12}H$, 1261.7415; found 1261.7481 (Supplementary Data 7,8).

Synthesis of L^2Ni_2

A solution of nickel(II) acetate tetrahydrate (13.7 mM in methanol, 4.2 mL, 58 μmol) was added to a solution of H_4L^2 (36.1 mg, 28.6 μmol) in chloroform (9.8 mL). The reaction mixture was left to stand for 6 h at room temperature and concentrated to dryness. The residue was washed several times with methanol and the product was collected by centrifugation to yield L^2Ni_2 (27.9 mg, 20.3 μmol, 71%) as dark red crystals. ^{1}H NMR (400 MHz, $CDCl_3$): δ 7.97 (s, 4H), 7.06 (s, 4H), 7.01 (d, J = 7.7 Hz, 4H), 6.92 (d, J = 7.7 Hz, 4H), 6.52 (t, J = 7.7 Hz, 4H), 4.56 (s, 8H), 4.01 (t, J = 6.4 Hz, 8H), 1.83 (quint, J = 7.0 Hz, 8H), 1.48 (quint, J = 7.0 Hz, 8H), 1.39–1.27 (m, 32H), 0.89 (t, J = 6.5 Hz, 12H); HRMS (ESI-TOF) (m/z): [L^2Ni_2 + H]$^+$ calcd. for $C_{76}H_{96}N_4O_{12}Ni_2H$, 1375.5801; found, 1375.5879 (Supplementary Data 9).

Synthesis of *rot*-L^2Ni_2•G1•PF_6

A solution of nickel(II) acetate tetrahydrate (27 mM in methanol, 0.75 mL, 20 μmol) was added to a solution containing H_4L^2 (12.6 mg, 10 μmol) and **G1**•PF_6 (46.9 mg, 103 μmol) in chloroform (1.8 mL). The mixture was stirred at room temperature for 3 h and was concentrated dryness. The residue was suspended in methanol, collected on a filter, and thoroughly washed with methanol to obtain *rot*-L^2Ni_2•**G1**•PF_6 (13.6 mg, 7.4 μmol, 75%) as dark red crystals. ^{1}H NMR (600 MHz, $CDCl_3/CD_3CN$ (4:1)): δ 8.65 (br, 2H), 8.11 (s, 4H), 7.43 (d, J = 8.1 Hz, 4H), 7.14 (s, 4H), 7.11 (dd, J = 7.9, 1.4 Hz, 4H), 6.96 (d, J = 8.1 Hz, 4H), 6.82 (dd, J = 7.9, 1.4 Hz, 4H), 6.64 (t, J = 7.9 Hz, 4H), 5.26–5.24 (m, 4H), 4.07 (t, J = 6.5 Hz, 8H), 3.91 (s, 8H), 2.33 (t, J = 7.8 Hz, 4H), 1.85 (quint, J = 7.0 Hz, 8H), 1.50 (quint, J = 7.5 Hz, 8H), 1.42–1.25 (m, 36H), 1.21 (sext, J = 7.4 Hz, 4H), 0.89 (t, J = 7.0 Hz, 12H), 0.83 (t, J = 7.3 Hz, 6H); ESI-MS (*m/z*): $[L^2Ni_2$•**G1**$]^+$ calcd. for $C_{98}H_{128}N_5O_{12}Ni_2$, 1684.8270; found, 1684.8407 (Supplementary Data 10).

X-ray crystallography

The intensity data were collected on a Bruker SMART APEX II or a Bruker Venture diffractometer with Cu Kα radiation (λ = 1.54178 Å). The diffraction data were corrected for the Lorentz and polarization factors, and for absorption using the multi-scan methods. The structure was solved by direct methods (SHELXT[85]) and refined by full-matrix least squares on F^2 using SHELXL 2014[86]. The non-hydrogen atoms were refined anisotropically and hydrogen atoms were idealized using the riding models. The crystallographic data are summarized in Supplementary Tables S1 and S2. CCDC-2335486 (L^2Ni_2•$2CH_3CN$) (Supplementary Data 11) and −2335487 (*rot*-L^2Ni_2•**G1**•PF_6•5MeCN•$0.5H_2O$) (Supplementary Data 12) contain the supplementary crystallographic data for this paper.

Computational study

The DFT calculations were performed using the Gaussian09 packages[87] with the wB97XD functional and the 6-31 G(d,p) basis sets for C, H, N, O, and Ni. The geometry optimizations of *nthr*- and *rot*-L^1Ni_2•**G3**$^+$ starting from different conformations gave seven and five different structures, respectively, four of which are shown in Supplementary Figs. S10 and S11 (Supplementary Data 13–22). The relative stabilities are obtained after correction of the zero-point energies. The interaction energies were calculated by the supermolecule methods and the basis set superposition error (BSSE) was corrected using the counterpoise method. The energies for *nthr*- and *rot*-L^1Ni_2•**G3**$^+$ are summarized in the Supplementary Table S3.

Data availability

All data analyzed and generated throughout this study are included in this article and its accompanying Supplementary Information. The X-ray crystallographic data for structures reported in this article have been deposited at the Cambridge Crystallographic Data Centre (CCDC), under deposition number CCDC 2335486 and 2335487. These data can be obtained free of charge from The Cambridge Crystallographic Data Centre via www.ccdc.cam.ac.uk/data_request/cif.

Received: 29 February 2024; Accepted: 18 July 2024;
Published online: 31 July 2024

References

1. Amabilino, D. B. & Stoddart, J. F. Interlocked and intertwined structures and superstructures. *Chem. Rev.* **95**, 2725–2828 (1995).
2. Wenz, G., Han, B.-H. & Müller, A. Cyclodextrin rotaxanes and polyrotaxanes. *Chem. Rev.* **106**, 782–817 (2006).
3. Sauvage, J.-P. From chemical topology to molecular machines (Nobel lecture). *Angew. Chem. Int. Ed.* **56**, 11080–11093 (2017).
4. Stoddart, J. F. Mechanically interlocked molecules (MIMs)—molecular shuttles, switches, and machines (Nobel lecture). *Angew. Chem. Int. Ed.* **56**, 11094–11125 (2017).
5. Balzani, V., Credi, A., Raymo, F. M. & Stoddart, J. F. Artificial molecular machines. *Angew. Chem. Int. Ed.* **39**, 3348–3391 (2000).
6. Harada, A. Cyclodextrin-based molecular machines. *Acc. Chem. Res.* **34**, 456–464 (2001).
7. Schalley, C. A., Beizai, K. & Vögtle, F. On the way to rotaxane-based molecular motors: studies in molecular mobility and topological chirality. *Acc. Chem. Res.* **34**, 465–476 (2001).
8. Kim, K. Mechanically interlocked molecules incorporating cucurbituril and their supramolecular assemblies. *Chem. Soc. Rev.* **31**, 96–107 (2002).
9. Balzani, V., Credi, A. & Venturi, M. Light powered molecular machines. *Chem. Soc. Rev.* **38**, 1542–1550 (2009).
10. Stoddart, J. F. The chemistry of the mechanical bond. *Chem. Soc. Rev.* **38**, 1802–1820 (2009).
11. Erbas-Cakmak, S., Leigh, D. A., McTernan, C. T. & Nussbaumer, A. L. Artificial molecular machines. *Chem. Rev.* **115**, 10081–10206 (2015).
12. Xue, M., Yang, Y., Chi, X., Yan, X. & Huang, F. Development of pseudorotaxanes and rotaxanes: from synthesis to stimuli-responsive motions to applications. *Chem. Rev.* **115**, 7398–7501 (2015).
13. Thordarson, P., Bijsterveld, E. J. A., Rowan, A. E. & Nolte, R. J. M. Epoxidation of polybutadiene by a topologically linked catalyst. *Nature* **424**, 915–918 (2003).
14. Tachibana, Y., Kihara, N. & Takata, T. Asymmetric benzoin condensation catalyzed by chiral rotaxanes tethering a thiazolium salt moiety via the cooperation of the component: can rotaxane be an effective reaction field? *J. Am. Chem. Soc.* **126**, 3438–3439 (2004).
15. Osaki, M., Takashima, Y., Yamaguchi, H. & Harada, A. An artificial molecular chaperone: poly-*pseudo*-rotaxane with an extensible axle. *J. Am. Chem. Soc.* **129**, 14452–14457 (2007).
16. Leigh, D. A., Marcos, V. & Wilson, M. R. Rotaxane catalysts. *ACS Catal.* **4**, 4490–4497 (2014).
17. Neal, E. A. & Goldup, S. M. Chemical consequences of mechanical bonding in catenanes and rotaxanes: isomerism, modification, catalysis and molecular machines for synthesis. *Chem. Commun.* **50**, 5128–5142 (2014).
18. Pairault, N. & Niemeyer, J. Chiral mechanically interlocked molecules – applications of rotaxanes, catenanes and molecular knots in stereoselective chemosensing and catalysis. *Synlett* **29**, 689–698 (2018).
19. Pairault, N. et al. Heterobifunctional rotaxanes for asymmetric catalysis. *Angew. Chem. Int. Ed.* **59**, 5102–5107 (2020).
20. Kwamen, C. & Niemeyer, J. Functional rotaxanes in catalysis. *Chem. Eur. J.* **27**, 175–186 (2021).
21. Okumura, Y. & Ito, K. The polyrotaxane gel: a topological gel by figure-of-eight cross-links. *Adv. Mater.* **13**, 485–487 (2001).
22. Araki, J. & Ito, K. Recent advances in the preparation of cyclodextrin-based polyrotaxanes and their applications to soft materials. *Soft Matter* **3**, 1456–1473 (2007).
23. Harada, A., Hashidzume, A., Yamaguchi, H. & Takashima, Y. Polymeric rotaxanes. *Chem. Rev.* **109**, 5974–6023 (2009).
24. Vukotic, V. N. & Loeb, S. L. Coordination polymers containing rotaxane linkers. *Chem. Soc. Rev.* **41**, 5896–5906 (2012).
25. Koyama, Y. Synthesis of topologically crosslinked polymers with rotaxane-crosslinking points. *Polymer J.* **46**, 315–322 (2014).
26. Aoki, D. & Takata, T. Mechanically linked supramolecular polymer architectures derived from macromolecular [2]rotaxanes: synthesis and topology transformation. *Polymer* **128**, 276–296 (2017).
27. Sagara, Y. et al. Rotaxanes as mechanochromic fluorescent force transducers in polymers. *J. Am. Chem. Soc.* **140**, 1584–1587 (2018).
28. Sawada, J., Aoki, D., Otsuka, H. & Takata, T. A guiding principle for strengthening crosslinked polymers: synthesis and application of mobility-controlling rotaxane crosslinkers. *Angew. Chem. Int. Ed.* **58**, 2765–2768 (2019).
29. Mena-Hernando, S. & Pérez, E. M. Mechanically interlocked materials. Rotaxanes and catenanes beyond the small molecule. *Chem. Soc. Rev.* **48**, 5016–5032 (2019).
30. Takata, T. Switchable polymer materials controlled by rotaxane macromolecular switches. *ACS Cent. Sci.* **6**, 129–143 (2020).

31. Chen, L., Sheng, X., Li, G. & Huang, F. Mechanically interlocked polymers based on rotaxanes. *Chem. Soc. Rev.* **51**, 7046–7065 (2022).
32. Sauvage, J.-P. Transition metal-containing rotaxanes and catenanes in motion: toward molecular machines and motors. *Acc. Chem. Res.* **31**, 611–619 (1998).
33. Suzaki, Y., Taira, T., Osakada, K. & Horie, M. Rotaxanes and pseudorotaxanes with Fe-, Pd- and Pt-containing axles. Molecular motion in the solid state and aggregation in solution. *Dalton Trans.* **2008**, 4823–4833 (2008).
34. Crowley, J. D., Goldup, S. M., Lee, A.-L., Leigh, D. A. & McBurney, R. T. Active metal template synthesis of rotaxanes, catenanes and molecular shuttles. *Chem. Soc. Rev.* **38**, 1530–1541 (2009).
35. Beves, J. E., Blight, B. A., Campbell, C. J., Leigh, D. A. & McBurney, R. T. Strategies and tactics for the metal-directed synthesis of rotaxanes, knots, catenanes, and higher order links. *Angew. Chem. Int. Ed.* **50**, 9260–9327 (2011).
36. Lewis, J. E. M., Beer, P. D., Loeb, S. J. & Goldup, S. M. Metal ions in the synthesis of interlocked molecules and materials. *Chem. Soc. Rev.* **46**, 2577–2591 (2017).
37. Goswami, A., Saha, S., Biswas, P. K. & Schmittel, M. (Nano) mechanical motion triggered by metal coordination: from functional devices to networked multicomponent catalytic machinery. *Chem. Rev.* **120**, 125–199 (2020).
38. Gao, W.-X., Feng, H.-J., Guo, B.-B., Lu, Y. & Jin, G.-X. Coordination-directed construction of molecular links. *Chem. Rev.* **120**, 6288–6325 (2020).
39. Ogino, H. Relatively high-yield syntheses of rotaxanes. Syntheses and properties of compounds consisting of cyclodextrins threaded by α,ω-diaminoalkanes coordinated to cobalt(III) complexes. *J. Am. Chem. Soc.* **103**, 1303–1304 (1981).
40. Ogino, H. & Ohata, K. Syntheses and properties of rotaxane complexes. 2. Rotaxanes consisting of α- or β-cyclodextrin threaded by (μ-α,ω-diaminoalkane)bis[chlorobis(ethylenediamine)cobalt(III)] complexes. *Inorg. Chem.* **23**, 3312–3316 (1984).
41. Whang, D., Park, K.-M., Heo, J., Ashton, P. & Kim, K. Molecular necklace: quantitative self-assembly of a cyclic oligorotaxane from nine molecules. *J. Am. Chem. Soc.* **120**, 4899–4900 (1998).
42. Suzaki, Y. & Osakada, K. Formation, dynamic behavior, and chemical transformation of Pt complexes with a rotaxane-like structure. *Chem. Asian J.* **1**, 331–343 (2006).
43. Markies, P. R., Nomoto, T., Akkerman, O. S. & Bickelhaupt, F. X-ray structure of (1,3-xylyl-18-crown-5)diphenylmagnesium: an organometallic rotaxane. *J. Am. Chem. Soc.* **110**, 4845–4846 (1988).
44. Gruter, G.-J. M. et al. Formation of the first organometallic catenane. *J. Am. Chem. Soc.* **115**, 12179–12180 (1993).
45. Blight, B. A., van Noortwyk, K. A., Wisner, J. A. & Jennings, M. C. [2] Pseudorotaxanes through second-sphere coordination. *Angew. Chem. Int. Ed.* **44**, 1499–1504 (2005).
46. Blight, B. A., Wisner, J. A. & Jennings, M. C. Synthesis of a [2]rotaxane through first- and second-sphere coordination. *Chem. Commun.* **2006**, 4593–4595 (2006).
47. Yang, Y.-D. et al. Multicomponent self-assembled metal−organic [3] rotaxanes. *J. Am. Chem. Soc.* **137**, 12966–12976 (2015).
48. Sakata, Y., Nakamura, R., Hibi, T. & Akine, S. Speed tuning of the formation/dissociation of a metallorotaxane. *Angew. Chem. Int. Ed.* **62**, e202217048 (2023).
49. Jeong, K.-S., Choi, J. S., Chang, S.-Y. & Chang, H.-Y. Self-assembly of rotaxane-like complexes with macrocycles containing reversible coordination bonds. *Angew. Chem. Int. Ed.* **39**, 1692–1695 (2000).
50. Clever, G. H. & Shionoya, M. A pH switchable pseudorotaxane based on a metal cage and a bis-anionic thread. *Chem. Eur. J.* **16**, 11792–11796 (2010).
51. Huang, S.-L., Hor, T. S. A. & Jin, G.-X. Metallacyclic assembly of interlocked superstructures. *Coord. Chem. Rev.* **333**, 1–26 (2017).
52. Aizawa, T., Akine, S., Saiki, T., Nakamura, T. & Nabeshima, T. Rotaxane formation by an allosteric pseudomacrocyclic anion receptor utilising kinetically labile copper(I) coordination properties. *Dalton Trans.* **51**, 17277–17282 (2022).
53. Shi, B. et al. Platinum metallacycle-based molecular recognition: establishment and application in spontaneous formation of a [2] rotaxane with light-harvesting property. *Angew. Chem. Int. Ed.* **62**, e202305767 (2023).
54. Yoon, I., Narita, M., Shimizu, T. & Asakawa, M. Threading-followed-by-shrinking protocol for the synthesis of a [2]rotaxane incorporating a Pd(II)–salophen moiety. *J. Am. Chem. Soc.* **126**, 16740–16741 (2004).
55. Hirose, K., Shiba, Y., Ishibashi, K., Doi, Y. & Tobe, Y. An anthracene-based photochromic macrocycle as a key ring component to switch a frequency of threading motion. *Chem. Eur. J.* **14**, 981–986 (2008).
56. Hirose, K., Shiba, Y., Ishibashi, K., Doi, Y. & Tobe, Y. A shuttling molecular machine with reversible brake function. *Chem. Eur. J.* **14**, 3427–3433 (2008).
57. Hirose, K., Ishibashi, K., Shiba, Y., Doi, Y. & Tobe, Y. Highly effective and reversible control of the rocking rates of rotaxanes by changes to the size of stimulus-responsive ring components. *Chem. Eur. J.* **14**, 5803–5811 (2008).
58. Sakata, Y., Kobayashi, S. & Akine, S. Two-step modulation of ion recognition using a bis(saloph)-macrocyclic host having a 24-crown-8-like cavity. *Chem. Commun.* **53**, 6363–6366 (2017).
59. Ashton, P. R. et al. Dialkylammonium ion/crown ether complexes: the forerunners of a new family of interlocked molecules. *Angew. Chem., Int. Ed. Engl.* **34**, 1865–1869 (1995).
60. Ashton, P. R. et al. Pseudorotaxanes formed between secondary dialkylammonium salts and crown ethers. *Chem. Eur. J.* **2**, 709–728 (1996).
61. Glink, P. T., Schiavo, C., Stoddart, J. F. & Williams, D. J. The genesis of a new range of interlocked molecules. *Chem. Commun.* **1996**, 1483–1490 (1996).
62. Ashton, P. R. et al. Self-assembling [2]- and [3]rotaxanes from secondary dialkylammonium salts and crown ethers. *Chem. Eur. J.* **2**, 729–736 (1996).
63. Ashton, P. R. et al. Rotaxane or pseudorotaxane? That is the question! *J. Am. Chem. Soc.* **120**, 2297–2307 (1998).
64. Akine, S., Utsuno, F. & Nabeshima, T. Highly efficient regulation of cation recognition and promotion of self-assembly by metalation of a macrocyclic bis(N_2O_2) ligand with nickel(II). *Chem. Commun.* **46**, 1029–1031 (2010).
65. Akine, S. et al. Synthesis, ion recognition ability, and metal-assisted aggregation behavior of dinuclear metallohosts having a bis(saloph) macrocyclic ligand. *Inorg. Chem.* **55**, 810–821 (2016).
66. Akine, S., Miyashita, M., Piao, S. & Nabeshima, T. Perfect encapsulation of a guanidinium ion in a helical trinickel(II) metallocryptand for efficient regulation of the helix inversion rate. *Inorg. Chem. Front.* **1**, 53–57 (2014).
67. Akine, S., Miyashita, M. & Nabeshima, T. Enhancement of alkali metal ion recognition by metalation of a tris(saloph) cryptand having benzene rings at the bridgeheads. *Inorg. Chem.* **60**, 12961–12971 (2021).
68. Ikbal, S. A., Zhao, P., Ehara, M. & Akine, S. Acceleration and deceleration of chirality inversion speeds in a dynamic helical metallocryptand by alkali metal ion binding. *Sci. Adv.* **9**, eadj5536 (2023).
69. Martínez-Díaz, M.-V., Spencer, N. & Stodeart, J. F. The self-assembly of a switchable [2]rotaxane. *Angew. Chem. Int. Ed. Engl.* **36**, 1904–1907 (1997).
70. Kawasaki, H., Kihara, N. & Takata, T. High yielding and practical synthesis of rotaxanes by acylative end-capping catalyzed by tributylphosphine. *Chem. Lett.* **1999**, 1015–1016 (1999).
71. Thibeault, D. & Morin, J.-F. Recent advances in the synthesis of ammonium-based rotaxanes. *Molecules* **15**, 3709–3730 (2010).

72. Sato, H., Aoki, D. & Takata, T. Which one is bulkier: the 3,5-dimethylphenyl or the 2,6-dimethylphenyl group? Development of size-complementary molecular and macromolecular [2]rotaxanes. *Chem. Asian J.* **13**, 785–789 (2018).
73. Groppi, J. et al. Precision molecular threading/dethreading. *Angew. Chem. Int. Ed.* **59**, 14825–14834 (2020).
74. Ong, C. W., Liao, S.-C., Chang, T. H. & Hsu, H.-F. In situ synthesis of hexakis(alkoxy)diquinoxalino[2,3-*a*:2′,3′-*c*]phenazines: mesogenic phase transition of the electron-deficient discotic compounds. *J. Org. Chem*. **69**, 3181–3185 (2004).
75. Wu, K. et al. Rational design of D−π−A−π−D porous organic polymer with polarized π for photocatalytic aerobic oxidation. *Appl. Catal. B.* **334**, 122847 (2023).
76. Horn, M., Ihringer, J., Glink, P. T. & Stoddart, J. F. Kinetic versus thermodynamic control during the formation of [2]rotaxanes by a dynamic template-directed clipping process. *Chem. Eur. J.* **9**, 4046–4054 (2003).
77. Tokunaga, Y. et al. Do dibenzo[22–30]crown ethers bind secondary ammonium ions to form pseudorotaxanes? *Bull. Chem. Soc. Jpn.* **80**, 1377–1382 (2007).
78. Nakamura, T. et al. Rotaxanes comprising cyclic phenylenedioxydiacetamides and secondary mono- and bis-dialkylammonium ions: effect of macrocyclic ring size on pseudorotaxane formation. *Org. Chem. Front.* **7**, 513–524 (2020).
79. Hupatz, H. et al. Thermodynamic and electrochemical study of tailor-made crown ethers for redox-switchable (pseudo)rotaxanes. *Beilstein J. Org. Chem.* **16**, 2576–2588 (2020).
80. Chaudhry, M. T., Soto, M. A., Lelj, F. & MacLachlan, M. J. Diverse binding of cationic guests by highly substituted [3+3] Schiff-base macrocycles. *Org. Chem. Front.* **8**, 1437–1446 (2021).
81. Gaedke, M. et al. Dual-stimuli pseudorotaxane switches under kinetic control. *Org. Chem. Front.* **8**, 3659–3667 (2021).
82. Hua, K., Li, X. & Han, Y.-F. Synthesis and properties of cyclic tetracarbene-based organometallic assemblies. *J. Organomet. Chem.* **917**, 121250 (2020).
83. Li, Y. et al. Strategies for the construction of supramolecular assemblies from poly-NHC ligand precursors. *Sci. China Chem.* **64**, 701–718 (2021).
84. Yu, G., Suzaki, Y., Abe, T. & Osakada, K. Introduction of ferrocene-containing [2]rotaxanes onto siloxane, silsesquioxane and polysiloxanes *via* click chemistry. *Dalton Trans.* **42**, 1476–1482 (2013).
85. Sheldrick, G. M. *SHELXT* – integrated space-group and crystal-structure determination. *Acta Crystallogr.* **A71**, 3–8 (2015).
86. Sheldrick, G. M. Crystal structure refinement with *SHELXL*. *Acta Crystallogr.* **C71**, 3–8 (2015).
87. Gaussian 09, Revision C.01, Frisch, M. J. et al. Gaussian, Inc., Wallingford CT, 2009.

Acknowledgements

The research was partly supported by the Japan Society of the Promotion Science (KAKENHI Grants JP21H05477 and JP23H04021 [Condensed Conjugation] as well as JP16H06510 [Coordination Asymmetry], JP18H03913, JP20K21206, and JP23H01972) and the World Premier International Research Initiative, Ministry of Education, Culture, Sports, Science and Technology, Japan. This paper is dedicated to professor Takayuki Kawashima on the occasion of his 77th birthday.

Author contributions

S.A. conceived and designed the research. S.K., M.Y., K.D., M.K., and S.Y. carried out the experimental work, analysis, and interpretation of the results. Y.S. and S.A. carried out the crystallographic analysis. Y.S. and S.A. supervised the project and supported the analysis and interpretation of the results. All the authors discussed the results and edited the manuscript.

Competing interests

The authors declare no competing interests.

Additional information

Supplementary information The online version contains supplementary material available at https://doi.org/10.1038/s42004-024-01246-8.

Correspondence and requests for materials should be addressed to Shigehisa Akine.

Peer review information *Communications Chemistry* thanks the anonymous reviewers for their contribution to the peer review of this work.